Kinetic Studies of the Reactions $CH_3 + NO_2 \rightarrow$ Products, $CH_3O + NO_2 \rightarrow$ Products, and $OH + CH_3C(O)CH_3 \rightarrow CH_3C(O)OH + CH_3$, over a Range of Temperature and Pressure

Matthias Wollenhaupt and John N. Crowley*

Max-Planck-Institut für Chemie, Division of Atmospheric Chemistry, Postfach 3060, 55020 Mainz, Germany

Received: February 11, 2000; In Final Form: April 5, 2000

The title reactions were investigated using pulsed laser photolysis combined with pulsed laser induced fluorescence detection of CH_3O to determine the rate coefficients for $CH_3 + NO_2 \rightarrow$ products (3) and $CH_3O + NO_2 \rightarrow$ products (5) as a function of temperature and pressure, and to estimate the yield of CH_3 (and thus the yield of $CH_3C(O)OH$) from the reaction of OH with $CH_3C(O)CH_3$ (2) at two different temperatures. Reaction 3 has both bimolecular and termolecular components: a simplified falloff parametrization with $F_{cent} = 0.6$ gives $k_{3b}^0 = (3.2 \pm 1.3) \times 10^{-28}(T/297)^{-0.3}$ cm^6 s^{-1} and $k_{3b}^\infty = (4.3 \pm 0.4) \times 10^{-11}(T/297)^{-1.2}$ cm^3 s^{-1} with CH_3NO_2 the likely product. The rate constant for the bimolecular reaction pathway to form $CH_3O + NO$ (3a) was found to be 1.9×10^{-11} cm^{-3} s^{-1}. The low- and high-pressure limiting rate coefficients for reaction between CH_3O and NO_2 to form CH_3ONO_2 (5b) were derived as $k_{5b}^0 = (5.3 \pm 0.3) \times 10^{-29}(T/297)^{-4.4}$ cm^6 s^{-1} and $k_{5b}^\infty = (1.9 \pm 0.05) \times 10^{-11}(T/297)^{-1.9}$ cm^3 s^{-1}, respectively. Although the final result is associated with some experimental uncertainty, we find that CH_3 is formed in the reaction between OH and $CH_3C(O)CH_3$ at ≈50% yield at room temperature and 30% at 233 K.

1. Introduction

A combination of field measurements and modeling studies has recently highlighted the important role of acetone ($CH_3C(O)CH_3$) in the chemistry of the upper troposphere, where it can contribute significantly to the concentration of HO*x*.[1−7] The major sink of $CH_3C(O)CH_3$ in the upper troposphere is photolysis, though the reaction with OH contributes significantly; in the lower troposphere this is reversed, and reaction with OH is the major sink:

$$CH_3C(O)CH_3 + h\nu \rightarrow CH_3C(O) + CH_3 \quad (1)$$

$$CH_3C(O)CH_3 + OH \rightarrow \text{products} \quad (2)$$

In a recent publication[8] we have shown that the overall rate coefficient, k_2, for reaction of OH with $CH_3C(O)CH_3$ does not display normal Arrhenius behavior, but that the temperature dependence, $k_2 = 8.8 \times 10^{-12} \exp(-1320/T) + 1.7 \times 10^{-14} \exp(423/T)$ cm^3 s^{-1}, can be explained if the reaction proceeds via two pathways, one of which has a positive activation barrier and the second an apparent negative activation barrier. We hypothesized that this was due to a change in reaction mechanism at low temperatures, where the initial step is electrophillic addition of OH to form an association complex, AC, of formula $(CH_3)_2C(OH)O$, that can dissociate to form acetic acid and the methyl radical (2a). At higher temperatures the reaction proceeds via H-atom abstraction (2b).

$$CH_3C(O)CH_3 + OH \rightarrow AC \rightarrow CH_3C(O)OH + CH_3 \quad (2a)$$

$$\rightarrow CH_3C(O)CH_2 + H_2O \quad (2b)$$

We further speculated that reaction 2a could represent a significant source of $CH_3C(O)OH$ in the upper troposphere (where cold temperatures favor its formation), and help explain recent observations of this species at high altitudes over the south Atlantic.[9] We note also that even at room temperature our analysis indicated that ≈40% of the reaction may proceed via channel 2a.

The estimation of the branching ratio to $CH_3C(O)OH$ based on the shape of the temperature dependence of the overall rate coefficient is clearly not unambiguous. Therefore, in the present study, we have carried out a series of experiments to confirm the presence of reaction pathway 2a and to quantify its contribution to the overall reaction of OH with $CH_3C(O)CH_3$ at different temperatures. As neither $CH_3C(O)OH$ or CH_3 can be detected by laser induced fluorescence (see below), we chose to scavenge any CH_3 formed in reaction 2 with NO_2 to generate CH_3O (which can be detected by pulsed laser induced fluorescence (PLIF)). Detailed experiments of the temperature and pressure dependence of the reactions of CH_3 and CH_3O with NO_2 were carried out to provide kinetic and mechanistic information necessary to analyze the CH_3O formation and decay in this system. The reaction of CH_3O with NO_2 has recently been identified as an important source of CH_3ONO_2 in the lower stratosphere,[10] although accurate estimation of the source strength was made difficult owing to the lack of kinetic data for this termolecular reaction at the appropriate pressure and temperature, which is remedied in the present experiments. In addition, we note that radical−radical reactions of the type $CH_3 + NO_2$ and $CH_3O + NO_2$ which have more than one reactive channel are of particular interest from both kinetic and dynamic standpoints.[11] An improved coverage of experimentally accessible parameter space (in this case, rate coefficients as a function of temperature and pressure) is needed to aid and exploit theoretical advances in the description of such reactions.

2. Experimental Section

The experiments were carried out using the method of pulsed laser photolysis combined with pulsed laser induced fluorescence (PLP−PLIF). Details of the experimental setup have been

10.1021/jp0005726 CCC: $19.00
Published on Web 06/16/2000

presented in a recent publication.[8] Briefly, CH_3O, generated in suitable precursor photochemistry initiated by the pulsed 193 or 351 nm radiation of an excimer laser, was excited at 292.8 nm (34 152 cm^{-1}, $A^2A_1 \leftarrow X^2E$, $v_3' = 4$)[12] and its red-shifted emission was detected with a photomultiplier (PMT) screened by an interference filter with maximum transmission at 330 nm and a bandwidth at half-maximum of 5.5 nm. The filter effectively shielded the PMT from scattered light from both the excitation laser (292.8 nm) and the photolysis laser (351 or 193 nm). The tunable excitation radiation was provided by frequency doubling the narrow-band emission from a dye laser (Rhodamine B), which was pumped at 532 nm using the second harmonic of a Nd:YAG laser operating at 10 Hz. The CH_3O excitation spectrum, measured by scanning the dye laser between 291 and 295 nm, showed qualitative agreement with that presented by Wantuck et al.[13] Time-resolved CH_3O profiles were measured by variation of the delay between the photolysis laser and the excitation laser, both running at 10 Hz. In practice, the Nd:YAG laser was triggered with a constant delay, and the excimer laser delay incremented relative to it after every laser pulse. This way a complete profile, consisting of 200 data points, was constructed in 20 s, and 20 scans were usually averaged to improve the signal-to-noise ratio. Generally 10−20 data points were also collected before the excimer laser pulse, which gives the background 292.8 nm scattered light intensity. A few percent of the excitation laser emission was beam split to a photodiode, and the signal obtained was used to normalize the fluorescence signal for pulse-to-pulse fluctuations in the intensity.

The experiments were carried out at pressures between 10 and 200 Torr of Ar (measured by 10, 100, and 1000 Torr capacitance manometers) and at temperatures between 223 and 356 K (determined by a J-type thermocouple inserted into the reaction volume). In a single experiment N_2 bath gas was also used. The total flow rate was regulated using calibrated mass flow controllers and varied between 40 and 450 cm^3 (STD) min^{-1} (sccm) depending on the total pressure. Acetone was stored as either a 5% or 5‰ mixture in Ar and introduced into the system via a flow controller. HONO was generated in situ by the reaction of HCl with $NaNO_2$ crystals (see below); CH_3ONO was introduced into the reactor from a 5% mixture in a 10 L blackened glass bulb via a Teflon needle valve. NO_2 was prepared as described below and stored at ≈5% dilution in Ar, in a blackened glass bulb. The dilute NO_2/Ar mixture was introduced into the reactor via mass flow controllers.

2.1. $OH + CH_3C(O)CH_3 \rightarrow CH_3 + CH_3C(O)OH$. The experiments can be broadly divided into two sets. In one set we probed the generation of $CH_3C(O)OH$ in reaction 2a, by monitoring the formation of its coproduct, CH_3, via a conversion reaction to CH_3O, which can be detected using PLIF.

$$OH + CH_3C(O)CH_3 \rightarrow CH_3C(O)OH + CH_3 \quad (2a)$$

$$CH_3 + NO_2 \rightarrow CH_3O + NO \quad (3a)$$

In these experiments, OH was formed in the 351 nm (excimer laser) photolysis of HONO (4) as described previously,[8] but

$$HONO + h\nu(351\ nm) \rightarrow OH + NO \quad (4)$$

was not detected. Relatively high concentrations of up to 10^{12} cm^{-3} OH were generated in order to maximize the concentration of CH_3 and consequently that of CH_3O. The concentration of OH generated this way was calculated from the 351 nm laser fluence (measured with a calibrated Joulemeter) and the concentration of HONO, which was determined by optical absorption in a 174 cm absorption cell located upstream of the photolysis reactor. The quantum yield for OH formation at 351 nm was taken to be unity;[8] the absorption cross section used was 1.83×10^{-19} cm^2.[14,15]

Detection of absorption between 205 and 370 nm using a 0.5 m monochromator equipped with a 1024 pixel diode array camera and a D_2 lamp as analysis light source enabled the concentrations of HONO, $CH_3C(O)CH_3$, and NO impurity to be measured simultaneously. Optical density measurements between 205 and 370 nm were converted to concentrations of NO, HONO, and $CH_3C(O)CH_3$ by least-squares fitting to reference spectra that had been obtained in the same setup (NO and $CH_3C(O)CH_3$[8]) or to a literature spectrum (HONO[14,15]). For NO, a non-Beer−Lambert relationship between the measured optical density and the NO concentration was observed, due to spectrally unresolved γ-bands. This was taken into account when calculating the NO concentration.

The analysis of the CH_3O profiles thus obtained required kinetic data for the reactions of both CH_3 with NO_2 and CH_3O with NO_2 at the pressures and temperatures of these experiments.

2.2. $CH_3 + NO_2 \rightarrow$ Products, $CH_3O + NO_2 \rightarrow$ Products. In a second set of experiments we conducted a detailed study of the reactions of CH_3 and CH_3O with NO_2:

$$CH_3 + NO_2 \rightarrow CH_3O + NO \quad (3a)$$

$$CH_3 + NO_2 + M \rightarrow CH_3NO_2 + M \quad (3b)$$

$$CH_3O + NO_2 \rightarrow HCHO + HONO \quad (5a)$$

$$CH_3O + NO_2 + M \rightarrow CH_3ONO_2 + M \quad (5b)$$

In these experiments, CH_3 radicals were generated by the 193 nm photolysis of acetone (6), which forms two CH_3 radicals.[16]

$$CH_3C(O)CH_3 + h\nu(193\ nm) \rightarrow 2CH_3 + CO \quad (6)$$

We note that CH_3 is vibrationally excited[17] in v_3 when formed from acetone photolysis at 193 nm (v_3 = 1:2:3 = 0.73:0.14:0.13). The rate coefficient for vibrational deactivation by Ar is 6.8×10^{-13} cm^3 s^{-1}. At the lowest pressure of these experiments (10 Torr), this corresponds to a relaxation lifetime of ≈4 μs, which is much shorter than the lifetime of CH_3 due to reaction with NO_2 (see below).

The sensitivity of the setup to CH_3O was determined by the photolysis of CH_3ONO at 351 nm (7). Measurement of the laser

$$CH_3ONO + h\nu(351\ nm) \rightarrow CH_3O + NO \quad (7)$$

fluence using a calibrated Joulemeter, and the concentration of CH_3ONO, measured by optical absorption, allowed the amount of CH_3O generated in the laser-irradiated volume to be calculated. The CH_3ONO concentration in these experiments was derived by least-squares fitting of the optical absorption between 300 and 360 nm to a reference spectrum measured using the same absorption cell. The cross section at the photolysis wavelength (351 nm) was determined to be 3.31×10^{-19} cm^2, which is in good agreement with literature values.[18] The quantum yield for CH_3O formation at wavelengths close to 350 nm has been determined as approximately unity.[19]

2.3. Chemicals. CH_3ONO was synthesized by the dropwise addition of 50% H_2SO_4 to an aqueous solution of $NaNO_2$ and CH_3OH, and carried in a stream of He into a cold trap at −78 °C. HONO was prepared in a dynamic flow system by passing HCl over a stirred bed of $NaNO_2$ crystals. HONO made this way contains high levels of NO impurity.[8] NO_2 was prepared by mixing pure NO with a large excess of O_2, which was then

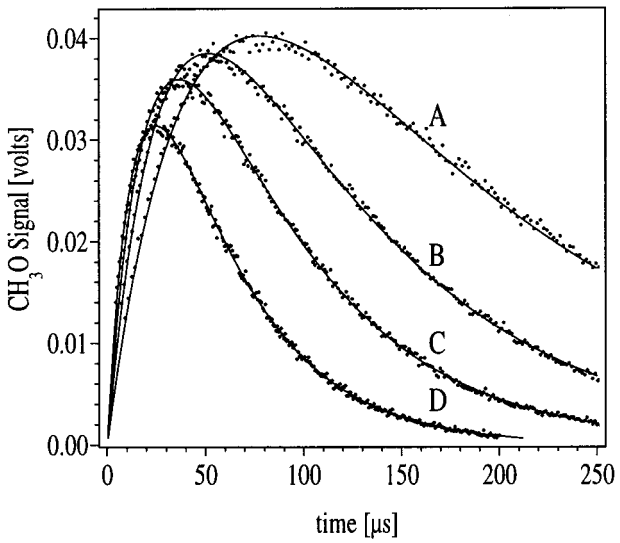

Figure 1. CH_3O profiles in the 193 nm photolysis of $CH_3C(O)CH_3$ in the presence of various excess concentrations of NO_2. The temperature was 233 K and the total pressure was 200 Torr Ar. A, $[NO_2] = 2.84 \times 10^{14}$ cm^{-3}; B, $[NO_2] = 4.40 \times 10^{14}$ cm^{-3}; C, $[NO_2] = 6.13 \times 10^{14}$ cm^{-3}; D, $[NO_2] = 9.24 \times 10^{14}$ cm^{-3}.

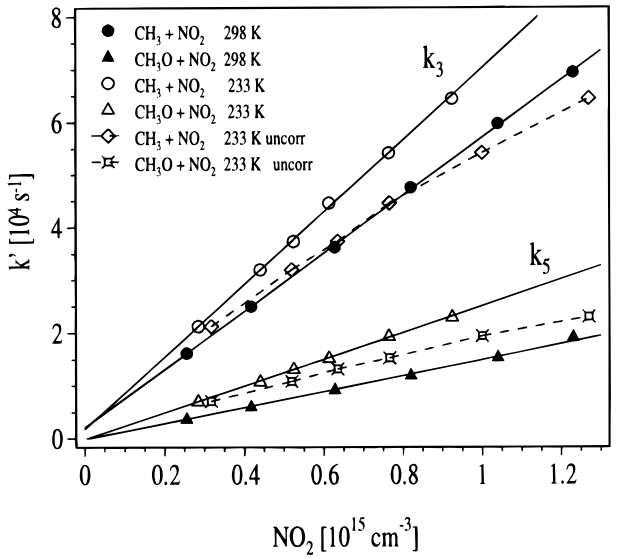

Figure 2. Plot of k'_3 and k'_5 versus $[NO_2]$ at 200 Torr of total pressure and at 233 and 298 K. The data joined with the dashed line have not been corrected to take into account the dimerization of NO_2.

removed by vacuum distillation. The NO_2 prepared this way typically had a NO impurity of 1%. NO, purchased at 99.5% purity (Matheson), was passed through a silica gel column at −78 °C to remove higher oxides. Ar and N_2 (Linde 99.999%) were used without further purification.

3. Results and Discussion

3.1. $CH_3 + NO_2$ and $CH_3O + NO_2$. The above reactions were studied simultaneously by photolyzing acetone at 193 nm in the presence of NO_2. Experimental conditions were chosen so that NO_2 was in great excess over the CH_3 radical. Typically, acetone at concentrations of $\approx 1 \times 10^{14}$ cm^{-3} was dissociated with a laser fluence of $\approx$0.5 mJ /cm^2 to give initial CH_3 concentrations of $[CH_3]_0 \approx 3 \times 10^{11}$ cm^{-3}, calculated using an acetone cross section of 2.7×10^{-18} cm^2. [20] The NO_2 concentration was varied between $\approx$0.2 and 1.2×10^{15} cm^{-3}. Under these conditions the self-reaction of CH_3 radicals is negligible, and reactions of CH_3 or CH_3O with secondary products or impurities (e.g., NO) are insignificant. The time-dependent CH_3O concentration profile is given by

$$[CH_3O]_t = \frac{k'_{3a}}{k'_5 - k'_3}(e^{-k'_3 t} - e^{-k'_5 t})[CH_3]_0 \qquad \text{(i)}$$

where k'_i is equal to $k_i[NO_2]$.

Time-dependent CH_3O profiles obtained in this manner and for different initial $[NO_2]$ are displayed in Figure 1. The variation in the maximum height of the CH_3O signal with $[NO_2]$ is due to quenching of the fluorescence by NO_2. The CH_3O profiles were fit to eq i to obtain k'_3 and k'_5 for a given temperature, pressure, and bath gas. The individual rate coefficients k_3 and k_5 are obtained by plotting k'_3 and k'_5 versus $[NO_2]$ as shown in Figure 2 for data obtained at 200 Torr and at 233 and 298 K. We note that for k_5 the intercept does not deviate from zero within statistical uncertainty. However, the data for k_3 display a positive intercept of between 1100 and 2200 s^{-1}, with no systematic dependence on either the temperature or pressure of the experiment. The lack of variation with pressure rules out that diffusion from the reaction zone (usually a maximum of $\approx$200 s^{-1}) or an effect related to vibrational excitation of CH_3 contributes significantly. Reactions of CH_3 in the absence of NO_2 (i.e., self-reaction or with acetone) are negligibly slow, and would in any case be expected to display a pressure and/or temperature dependence. Also, the simultaneous formation of O-atoms formed in the photolysis of NO_2 was considered as a potential source of error. However, although $\approx 1 \times 10^{11}$ O-atoms cm^{-3} (both $O(^1D)$ and $O(^3P)$) are generated in the laser pulse (for experiments with high NO_2), the fate of $O(^3P)$ will be reaction with NO_2 rather than with CH_3 or $CH_3C(O)CH_3$. The $O(^1D)$ generated could react with $CH_3C(O)CH_3$ to form OH radicals, though the fact that data obtained in Ar and N_2 give the same results suggests that any secondary chemistry related to $O(^1D)$ formation has no significant influence on the CH_3 or CH_3O profiles. At present we have no explanation for this apparent nonzero loss rate for CH_3 in the absence of NO_2 but note that it is small, and probably does not significantly influence the derivation of the rate coefficients for k_3.

The accuracy of the rate coefficients obtained in this study was enhanced by measuring the concentration of NO_2 by optical absorption in the 174 cm cell. Measurements of absorbance were converted to concentrations by least-squares fitting to a reference spectrum (310−365 nm) measured in the same setup and with the same instrumental resolution. The reference spectrum showed good agreement with the spectrum previously determined in this laboratory.[21] In addition, NO_2 was monitored after the reaction vessel by its absorption of the broad band emission of a light-emitting diode (LED, 410−440 nm) over a 44 cm path length. An effective cross section was established relative to absorption in the 174 cm cell, which allowed us to check that no NO_2 was lost in transit through the thermostated reaction vessel. The 174 and 44 cm absorption cells were at room temperature. The optically determined NO_2 concentration in the 174 cm cell was then corrected for pressure and temperature differences between the absorption cell and the reaction vessel to obtain its concentration. At temperatures of 262, 297, and 356 K the concentration of NO_2 is known to within 5%. At the lowest temperatures of this study 233 K, a further correction to the NO_2 concentration had to be made due to its dimerization to N_2O_4.

$$2NO_2 \leftrightarrow N_2O_4 \qquad (8,-8)$$

TABLE 1: Rate Coefficients for $CH_3 + NO_2 \rightarrow$ Products[a]

	temperature (K)			
pressure (Torr)	233	262	297	356
10	4.56[b]	4.25 ± 0.07	3.84 ± 0.09	3.43 ± 0.10
	4.09[c]			
20	5.21[b]	4.67 ± 0.12	4.41 ± 0.20	3.95 ± 0.10
	4.72[c]			
50	5.97[b]	5.77 ± 0.14	5.10 ± 0.07	4.50 ± 0.09
	5.38[c]		5.01 ± 0.11[d]	
100	6.57[b]	6.25 ± 0.17	5.24 ± 0.16	4.72 ± 0.12
	5.84[c]			
200	6.85[b]	6.12 ± 0.16	5.49 ± 0.13	4.92 ± 0.14
	6.04[c]			

[a] Rate coefficients in units of 10^{-11} cm^3 s^{-1}. [b] Data corrected for NO_2 dimerization using $K_8 = 5.2 \times 10^{-29}$ exp(6782/T) cm^3. [c] Data corrected for NO_2 dimerization using $K_8 = 5.2 \times 10^{-29}$ exp(6643/T) cm^3.[22] For $T = 262$ K, the correction was of the order of just 1% and was therefore not carried out. [d] Value obtained in N_2 bath gas. Errors are statistical only (2σ).

TABLE 2: Rate Coefficients for $CH_3O + NO_2 \rightarrow$ Products[a]

	temperature (K)			
pressure (Torr)	233	262	297	356
10	12.7[b]	8.67 ± 0.02	5.56 ± 0.07	3.22 ± 0.06
	11.4[c]			
20	15.9[b]	11.6 ± 0.02	7.46 ± 0.18	4.48 ± 0.06
	14.4[c]			
50	20.0[b]	15.8 ± 0.02	10.8 ± 0.01	6.57 ± 0.08
	18.1[c]		11.0 ± 0.10[d]	
100	22.6[b]	18.0 ± 0.03	13.2 ± 0.2	7.64 ± 0.11
	20.1[c]			
200	25.3[b]	19.0 ± 0.03	15.1 ± 0.2	9.48 ± 0.16
	22.3[c]			

[a] Rate coefficients in units of 10^{-12} cm^3 s^{-1}. [b] Data corrected for NO_2 dimerization using $K_8 = 5.2 \times 10^{-29}$ exp(6782/T) cm^3. [c] Data corrected for NO_2 dimerization using $K_8 = 5.2 \times 10^{-29}$ exp(6643/T) cm^3.[22] For $T = 262$ K, the correction was of the order of just 1% and was therefore not carried out. [d] Value obtained in N_2 bath gas. Errors are statistical only (2σ).

Initially the recommended equilibrium constant, $K_8 = 5.2 \times 10^{-29}$ exp((6643 ± 250)/T) cm^3, was used.[22] At the highest NO_2 concentrations employed ($[NO_2] = 1 \times 10^{15}$ cm^{-3} and at 223 K ($K_8 = 1.25 \times 10^{-16}$ cm^3 molecule^{-1}) the correction applied is ≈25%, which reduces to ≈5% at $NO_2 = 2 \times 10^{14}$ cm^{-3}. Using the recommended forward and backward rate coefficients for (8,−8),[23] we calculate that the relaxation time to reach equilibrium between NO_2 and N_2O_4 is <1 s even at the lowest pressures (10 Torr) and the lowest NO_2 concentrations. The residence time for the flowing gas mixture in the cooled part of the reactor is >4 s. The correction for dimerization of NO_2 removes the curvature present in plots of k' versus $[NO_2]$ at low temperatures as seen in Figure 2.

Data obtained for k_3 and k_5 at various pressures between 10 and 200 Torr and at various temperatures between 223 and 356 K are listed in Tables 1 and 2. The rate coefficients obtained for k_3 and k_5 were found to be independent of the excimer laser fluence and thus initial $[CH_3]$ when varied over a factor of 3, and independent of the flow rate and residence time of the flowing gas mixture in the reaction vessel. The data also showed no dependence on the time resolution used to measure the CH_3O profile, which suggested that sufficient data points were gathered to determine the rate of the rapid part of the CH_3O formation at short times.

The temperature- and pressure-dependent rate coefficients are also plotted in Figure 3 (for the reaction of CH_3O with NO_2) and Figure 4 ($CH_3 + NO_2$). The complete data set (i.e., all rate coefficients at each pressure and temperature) for each reaction was fitted simultaneously to falloff curves[24] described by

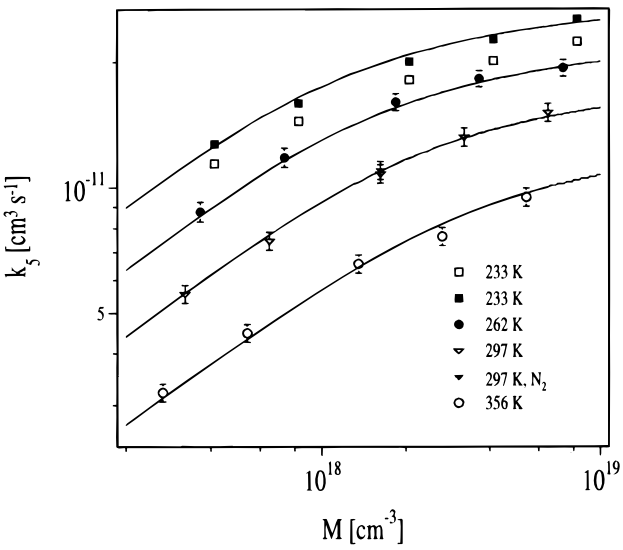

Figure 3. Falloff curves for $CH_3O + NO_2$. The data at 262, 297, and 356 K were fitted simultaneously to eq ii as described in the text. The rate constants at 233 K were corrected for the dimerization of NO_2 to form N_2O_4. The open squares were corrected using $K_8 = 5.2 \times 10^{-29}$ exp(6643/T) cm^3; the solid squares were corrected using $K_8 = 5.2 \times 10^{-29}$ exp(6782/T) cm^3.

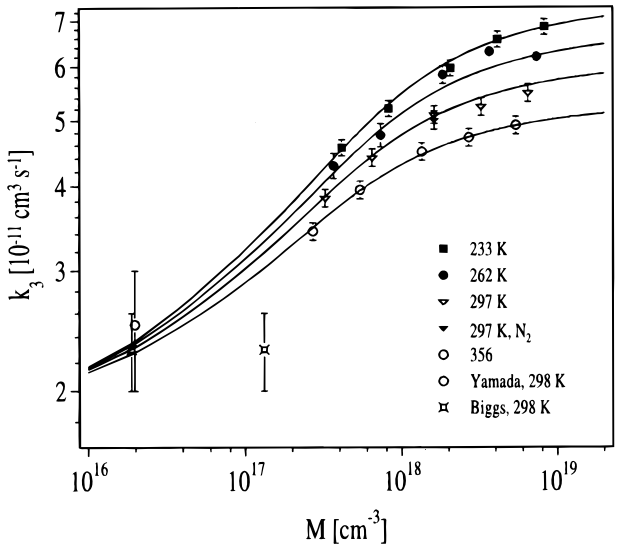

Figure 4. Falloff curves for $CH_3 + NO_2$. The data at 262, 297, and 356 K were fitted simultaneously to eq ii as described in the text. The solid lines are described by $F_{cent} = 0.6$, $k_0 = 3.18 \times 10^{-28}$ cm^6 s^{-1}, $k_\infty = 4.34 \times 10^{-11}$ cm^3 s^{-1}, $n = 0.3$, $m = 1.17$, and $k_{3a} = 1.91 \times 10^{-11}$ cm^3 s^{-1}. The rate constants at 233 K were corrected for the dimerization of NO_2 to form N_2O_4 using 5.2×10^{-29} exp(6782/T) cm^3. Low-pressure flow tube measurements in He are also shown: Yamada = ref 30; Biggs = ref 26. To allow direct comparison, the data obtained in He have been assigned an equivalent pressure of Ar to reflect the relative third-body efficiencies of these bath gases.

$$k(M,T) = \left(\frac{k_0\left(\frac{T}{297}\right)^{-n}[\mathrm{M}]}{1 + \left(k_0\left(\frac{T}{297}\right)^{-n}[\mathrm{M}]/k_\infty\left(\frac{T}{297}\right)^{-m}\right)} \right)(F_{cent})^p \quad \text{(ii)}$$

where k_0 is the low-pressure termolecular rate coefficient, k_∞ is the limiting high-pressure rate coefficient, $F_{cent} = \exp(-T/f)$, which describes the temperature-dependent broadening of the

falloff curves, and

$$p = \left\{1 + \left(\frac{\log_{10}\left(k_0\left(\frac{T}{297}\right)^{-n}[\mathrm{M}]\right)}{k_\infty\left(\frac{T}{297}\right)^{-m}}\right)^2\right\}^{-1}$$

3.1.1. $CH_3O + NO_2$. For the reaction of CH_3O with NO_2, a minor, bimolecular channel (5a) has been measured along with the pressure-dependent association reaction 5b.[25] In that work, k_{5a} was measured as $k_{5a}(T) = 9.6 \times 10^{-12} \exp(-1150/T)$ cm^3 s^{-1}, albeit with relatively large errors associated with both the preexponential factor and the temperature dependence. For this reason the present data was fitted to an equation of the form $k_5 = k_{5a}(T) + k_{5b}(M,T)$. Note that neglecting the bimolecular component (5a) would result in only small changes in the fits, as its contribution to the overall rate coefficient at the higher pressures of this experiment is small. The maximum effect is found at high temperatures and low pressures, e.g., $k_{5a}/k_{5b} \approx 0.1$ at 10 Torr and 356 K, and <0.01 at 10 Torr and 233 K. Potential energy surfaces showing the energetics of the various reaction pathways have been given by Biggs et al.[26]

Our initial calculations showed that the data at 356, 297, and 262 K could be well reproduced, but the fit overestimated the measured rate coefficients at 233 K. This is apparent in Figure 3, which displays the rate constant corrected as above for the dimerization of NO_2 using the recommended equilibrium constant (open squares). By fitting to the data at 262, 297, and 356 K only, we obtain the fits in Figure 3, which are described by $f = (571 \pm 112)$, $k_0 = (5.5 \pm 1.1) \times 10^{-29}$ cm^6 s^{-1}, $k_\infty = (1.86 \pm 0.06) \times 10^{-11}$ cm^3 s^{-1}, $n = (3.42 \pm 0.36)$, and $m = (1.80 \pm 0.14)$. A small adjustment to the temperature dependence of the equilibrium constant for the dimerization of NO_2 to N_2O_4 ($K_8 = 5.2 \times 10^{-29} \exp(6782/T)$ cm^3) brings our 223 K data back in line with this parametrization of the rate coefficient (solid squares in Figure 3). Note that this value of K_8 is well within the quoted error limits for the temperature dependence of the equilibrium constant.

The value of f obtained converts to values of F_{cent} of 0.66 at 223 K, decreasing to 0.55 at 356 K, reflecting the expected increase in the broadening factor as the temperature decreases. Note that the temperature dependence of F_{cent} was not forced in the fitting routine but was allowed to vary freely. If F_{cent} is held at 0.6, irrespective of the temperature,[22] we obtain $k_0 = (5.3\pm 0.3) \times 10^{-29}$ cm^6 s^{-1}, $k_\infty = (1.86 \pm 0.05) \times 10^{-11}$ cm^3 s^{-1}, $n = (4.36 \pm 0.36)$, and $m = (1.87 \pm 0.15)$; i.e., only n, which describes the temperature dependence of the low-pressure, third-order rate constant, is significantly changed, although there is no discernible difference in the quality of the fit.

In Figure 5, we compare our results with previous determinations of the pressure and temperature dependence of the rate coefficient. The solid lines are the calculated overall rate constant k_5, which was obtained using the parametrization of the termolecular component (in Ar) as described above, plus the bimolecular component as described by McCaulley et al.[25] The temperatures were chosen to match the available literature data. The data that were obtained in He have been corrected for the relative third-body efficiencies of He and Ar (β_c(He) = 0.07 and β_c(Ar) = 0.12) as determined in the experiments of Frost et al.[27]

McCaulley et al.[25] measured the rate coefficients between 0.6 and 4.0 Torr of He and $T = 220-473$ K using a low-pressure flow tube and detection of CH_3O with LIF. They also used the reaction $CH_3 + NO_2 \rightarrow CH_3O$ to generate CH_3O, but did not attempt to analyze the rise of CH_3O at short time to gain

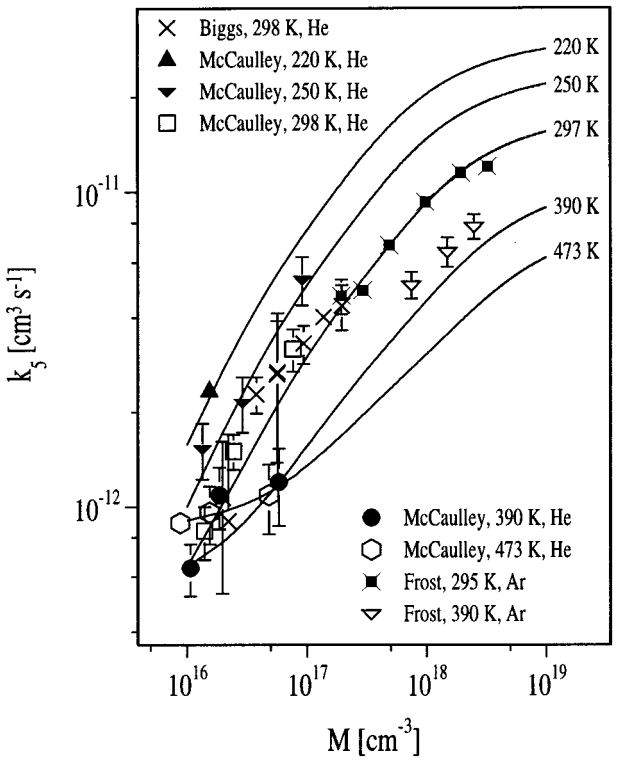

Figure 5. Comparison of present data for $CH_3O + NO_2$ with literature. The solid lines were calculated from the present parametrization of the termolecular component ($F_{cent} = 0.6$, $k_0 = 5.3 \times 10^{-29}$ cm^6 s^{-1}, $k_\infty = 1.86 \times 10^{-11}$ cm^3 s^{-1}, $n = 4.36$, $m = 1.87$) plus the temperature-dependent bimolecular component as measured by McCaulley et al. McCaulley = ref 25; Biggs = ref 26; Frost = ref 28. To allow direct comparison, the data obtained in He have been assigned an equivalent pressure of Ar to reflect the relative third-body efficiencies of these bath gases.

information concerning k_3. They obtained $k^0_{5a} = 2.6 \times 10^{-29}(T/300)^{-4.5}$ cm^6 s^{-1}, which compares well with the present determination of $n = 4.4$. A further low-pressure, flow tube study was conducted by Biggs et al.,[26] who monitored CH_3O profiles to extract both k_3 and k_5. Frost et al.[28] carried out flash photolysis experiments, using the photolysis of CH_3ONO as CH_3O source at pressures similar to those of the present study, and at 295 and 390 K.

The results obtained in those experiments generally show good agreement with the present parametrization of the rate coefficients. The data close to room temperature are in good agreement at all pressures; especially the flash photolysis data of Frost et al.[28] agree particularly well. The present parametrization of the rate coefficients is in good agreement with that obtained by Biggs et al.,[26] who derived $k_0 = (5.3 \pm 0.2) \times 10^{-29}$ cm^6 s^{-1} and $k_\infty = (1.43 \pm 0.03) \times 10^{-11}$ cm^3 s^{-1} with F_{cent} fixed at 0.6, by analysis of their own data at room temperature along with those of Frost et al.[28] and McCaulley et al.[25]

The low-pressure data of McCaulley et al.[25] at 220, 250, 390, and 473 K are also correctly reproduced. Some deviation is observed for the data of Frost et al.[28] at 390 K. The reason for this is unclear, and we can only speculate that it is related to the use of a different CH_3O precursor system than in the present experiments.

Although by far the most important loss process for CH_3O in the atmosphere is reaction with O_2, a combination of observations of CH_3ONO_2 in the lower stratosphere and upper troposphere and modeling studies[10] have led to the conclusion that ≈50% of the observed CH_3ONO_2 is formed in reaction

5b, with a further 50% provided by a minor channel ($\approx 10^{-5}$ of the overall rate coefficient) in the reaction of methylperoxy (CH_3O_2) with NO. The model used evaluated kinetic data on the reaction $CH_3O + NO_2$,[22] which returns a value of $k_{5b} = 2 \times 10^{-11}$ cm^3 s^{-1} for $T = 215$ K and 100 Torr. The value of k_{5b} at the same temperature and pressure from the present data is 3×10^{-11} cm^3 s^{-1}. Use of the present data to assess the sources of CH_3ONO_2 would therefore significantly reduce the extracted branching ratio for an additional channel to CH_3ONO_2 formation in the $CH_3O_2 + NO$ reaction.

3.1.2. $CH_3 + NO_2$. The data for this reaction were treated in a manner identical to that described above for k_5. That is, we fit the data at 233, 262, 297, and 356 K to eq ii with an additional bimolecular component, k_{3a}. In this case we initially assumed that the bimolecular channel (3a) does not have a strong temperature dependence,[29] so that $k_3 = k_{3a} + k_{3b}(M,T)$. Potential energy surfaces showing the energetics of the various reaction pathways have been given by Biggs et al.[26] The present data are displayed in Figure 4 (note that the data at 233 K have been corrected for NO_2 dimerization as described above). The simultaneous fit to all the data yields $f = (682 \pm 468)$, $k_0 = (2.64 \pm 1.7) \times 10^{-28}$ cm^6 s^{-1}, $k_\infty = (4.24 \pm 0.36) \times 10^{-11}$ cm^3 s^{-1}, $n = -(0.47 \pm 0.64)$, $m = (1.12 \pm 0.12)$, and $k_{3a} = 1.96 \times 10^{-11}$ cm^3 s^{-1}. F_{cent} is thus seen to decrease from 0.71 at 233 K to 0.59 at 356 K. If F_{cent} is held at 0.6, irrespective of the temperature,[22] we obtain $k_0 = (3.18 \pm 1.3) \times 10^{-29}$ cm^6 s^{-1}, $k_\infty = (4.34 \pm 0.4) \times 10^{-11}$ cm^3 s^{-1}, $n = (0.30 \pm 0.6)$, $m = (1.17 \pm 0.1)$, and $k_{3a} = 1.91 \times 10^{-11}$ cm^3 s^{-1}. Also plotted in Figure 4 are data obtained at low pressure by Yamada et al.[30] and Biggs et al.[26]

Yamada et al.[30] obtained a value of $k_{3a} = 2.5 \times 10^{-11}$ cm^3 s^{-1} at 295 K in flow tube experiments at 295 K and at pressures of 1 Torr with direct detection of CH_3 using photoionization mass spectrometry. Within the quoted error limits, this is in good agreement with the present extrapolation to 1 Torr (see Figure 4). Nitromethane (CH_3NO_2) was not observed in those experiments, indicating that channel 3b was not important at that pressure. This observation disagrees with the results of McCaulley et al.,[31] who measured yields of CH_3NO_2 of 0.04 at 298 K and a total pressure of 0.5 Torr of He, increasing to 0.07 at 1 Torr of He. They found no temperature dependence of the CH_3NO_2 yield at 1 Torr between 223 and 298 K.

In further flow tube experiments at pressures of 1−10 Torr of He, with LIF detection of CH_3O to follow the CH_3 kinetics, Biggs et al.[26] derived values for k_3 and k_5. They found k_3 to be independent of pressure between 1 and 7 Torr, with a rate constant of $(2.3 \pm 0.3) \times 10^{-11}$ cm^3 s^{-1}. Although the result at 1 Torr is in good agreement with the present data set, the lack of a pressure dependence is not commensurate with the present study, which revealed a pronounced pressure dependence at room temperature. A partial explanation for this difference may be related to the use of a low-pressure flow tube to determine the kinetics of a fast process ($CH_3 + NO_2$) and a significantly slower process ($CH_3O + NO_2$) simultaneously. Close examination of the data presented by these authors shows that the raw data are not accurately described by the fit to eq i, and that the resulting scatter in the plot of k' versus [NO_2] encompasses rate constants between 3.3 and 1.5×10^{-11} cm^3 s^{-1}. This may be related to problems with spatial resolution in the flow tube when attempting to measure first-order decay rates of close to 2000 s^{-1} and to heterogeneous loss of CH_3 and/or CH_3O on the flow tube walls. Glänzer and Troe[29] determined values for k_{3a} and k_{3b} in shock-tube studies at 900−1400 K at pressures between 1 and 30 atm. They determined $k_{3a} = 2.16 \times 10^{-11}$ cm^3 s^{-1} (for 1100−1400 K). For the termolecular channel they quote a high-pressure second-order limit of $k_3^\infty = 1.66 \times 10^{-11}(T/1000)^{-0.6}$ cm^6 s^{-1} between 300 and 1400 K, which yields a value of $k_3^\infty = 3.4 \times 10^{-11}$ cm^3 s^{-1} at 298 K, in reasonable agreement with the present result. For the low-pressure, third-order limit they obtained $k_3^0 = 6.9 \times 10^{-31}(T/1000)^{-6}$ cm^3 s^{-1}, which gives a value of 9.9×10^{-28} cm^6 s^{-1} at 298 K.

The present data indicate that the reaction between CH_3 and NO_2 displays a pronounced pressure dependence, and that the termolecular reaction pathway is important even at low pressures and dominant at pressures greater than ≈20 Torr of Ar. Note that, in the present experiments, the product(s) of the termolecular channel was (were) not detected. By analogy with previous low-pressure studies of the reactions of alkyl radicals with NO_2, we assume that CH_3NO_2 is formed, though we cannot rule out stabilization of CH_3ONO^* to form CH_3ONO at the higher pressures and low temperatures used in this study.

We derive a bimolecular, pressure-independent rate coefficient at 298 K of $k_{3a} = 1.9 \times 10^{-11}$ cm^3 s^{-1} and note that our parametrization of the reaction reproduces the low-pressure data of Yamada et al.[30] and Biggs et al.[26] If we extrapolate our results to 1 Torr, we obtain a ratio $k_{3b}/k_3 = 0.23$ at 298 K, increasing to 0.31 at 223 K. These values are significantly higher than the measurements of McCaulley et al.,[31] whose yields of CH_3NO_2 were between 4% and 7%. Some of this discrepancy will be related to the use of He as bath gas in the experiments of McCaulley et al., which is a less efficient third-body collisional quencher (by a factor of ≈0.6 for $CH_3O + NO_2$) than Ar. Investigations of the reaction of C_2H_5 with NO_2 at 300 K[32] with detection of $C_2H_5NO_2$ and NO products from the termolecular and bimolecular pathways, respectively, have resulted in a ratio of termolecular to bimolecular components of ≈0.25 between 0.7 and 2.1 Torr of He, in line with the present results for $CH_3 + NO_2$ when extrapolated to low pressures.

The difference between the present observations of a strong pressure dependence in the reaction of CH_3 and NO_2 and the literature data may reflect the fact that the previous measurements were not carried out over extended pressure ranges, and that the effect at low pressures is partially disguised by the presence of the fast, pressure independent bimolecular reaction, (3a). There are no temperature-dependent rate coefficients for $CH_3 + NO_2$ at low pressures (close to 1 Torr) available. The global fits to our data were of the form $k_3 = k_{3a} + k_{3b}(M,T)$ and were thus forced to return a temperature-independent rate constant for k_{3a}, which was found to be 1.91×10^{-11} cm^3 s^{-1}. The applicability of this assumption was tested by carrying out experiments at two temperatures, 297 and 255 K, at constant pressure (20 Torr). In such experiments, a variation in the rate constant for k_{3a} with temperature will be manifest as a change in the height of the CH_3O signal as the efficiency of CH_3O formation changes. The experiments were carried out back-to-back and in swift succession so that experimental parameters such as the fluence of both the photolysis laser and the excitation laser remained largely unchanged. The profiles obtained at each temperature were scaled for changes in $CH_3C(O)CH_3$ and thus CH_3 due to density changes as the gas mixture was cooled. The concentration of NO_2 in the absorption cell was monitored, and its concentration in the reaction vessel was calculated as usual. The data were then simulated using the parametrized rate constants given above for k_3 and k_5. For both temperatures, not only the shape but also the height of the profiles were well reproduced when k_{3a} was held at 1.9×10^{-11} cm^3 s^{-1}, which rules out a *strong* temperature dependence in k_{3a}. Within

TABLE 3: Experimental Conditions for the Investigation of Reaction 2[a]

expt	T	$CH_3C(O)CH_3$	HONO	NO_2	NO	OH	$O(^3P)$
11	233	9.7×10^{15}	2.0×10^{14}	1.6×10^{14}	6.8×10^{13}	1.3×10^{12}	2.3×10^{12}
13	233	3.9×10^{15}	1.8×10^{14}	2.0×10^{14}	9.2×10^{13}	1.2×10^{12}	2.9×10^{12}
15	233	8.2×10^{15}	2.5×10^{14}	3.3×10^{14}	1.2×10^{14}	1.7×10^{12}	4.8×10^{12}
6	297	7.0×10^{15}	1.4×10^{14}	2.6×10^{14}	9.8×10^{13}	9.4×10^{11}	3.9×10^{12}
7	297	7.4×10^{15}	1.5×10^{14}	1.6×10^{14}	8.2×10^{13}	1.0×10^{12}	2.4×10^{12}
8	297	3.4×10^{15}	1.5×10^{14}	1.6×10^{14}	8.8×10^{13}	1.0×10^{12}	3.9×10^{12}

[a] Temperature (T) in K. Concentrations in cm^{-3}. All experiments at 20 Torr of total pressure. OH and $O(^3P)$ concentrations are based on the measured laser fluence at 351 nm and on the absorption cross sections of HONO and NO_2 respectively, at this wavelength (in both cases a quantum yield of unity is assumed.). The NO_2 concentration at 233 K has been corrected for dimerization to form N_2O_4 (size of the correction was ≈ 10%). The NO concentration listed is that observed by optical absorption. This is incremented in the numerical simulation by the same concentration as $O(^3P)$, as both are formed in the dissociation of NO_2.

experimental uncertainty, we can place an upper limit of $E/RT = -300/T$ for the temperature dependence of k_{3a}.

3.2. OH + $CH_3C(O)CH_3$ → CH_3 + $CH_3C(O)OH$. This reaction was investigated by photolyzing HONO in the presence of $CH_3C(O)CH_3$ and NO_2 and by following the formation and decay of CH_3O by LIF. The main aim of these experiments was to quantify the branching ratio to CH_3 formation in reaction 2, and thus an absolute determination of CH_3O was necessary. For this reason, directly prior to the experiments, the sensitivity of the LIF detection scheme to CH_3O was measured. This was carried out by 351 nm photolysis of a known concentration of CH_3ONO at a known laser fluence (typically ≈20 mJ/cm^2) and, most importantly, in the presence of the same concentration of acetone to be used in the studies of the OH + acetone reaction. It was found that the sensitivity to CH_3O was severely degraded in the presence of $\approx(3-7) \times 10^{15}$ cm^{-3} of acetone due to fluorescence quenching. Such high concentrations of $CH_3C(O)CH_3$ were necessary to ensure that a high proportion of the OH formed reacted with the $CH_3C(O)CH_3$ and not with HONO or NO_2. Optical measurements of both acetone and CH_3ONO revealed no reactivity between these two molecules. Also, variation of the CH_3ONO concentration made no significant change in the sensitivity to CH_3O, implying that at concentrations of $\approx 1 \times 10^{14}$ cm^{-3} the CH_3ONO did not significantly quench the CH_3O fluorescence. The dye laser and excimer laser fluences were constantly monitored to enable corrections to the calibration factor for the CH_3O concentration to be made if necessary.

Altogether six experiments were carried out at 233 and 298 K, using various reactant concentrations. The experimental conditions are listed in Table 3. Note that, with the exception of OH and $O(^3P)$, all concentrations were determined by optical absorption measurements. CH_3O profiles from such experiments are shown (for 297 K) in Figure 6. Due to the low signal, 200 scans over ≈20 min were made to improve the signal-to-noise ratio, with each data point normalized to the excitation laser fluence. A correction to each profile was also made to account for HONO fluorescence following excitation at 292.8 nm. In experiments with no $CH_3C(O)CH_3$ present, we observed a rapid drop in background signal directly after the excimer laser pulse, followed by a further slow decrease over several milliseconds. Analysis of the time dependence of this signal showed that it was due to the immediate removal of HONO by the 351 nm laser pulse and then by reaction of HONO with OH. We conclude therefore that HONO fluoresces weakly at ≈330 nm following excitation at 292.8 nm. Normally this weak signal would not be significant, but due to the low CH_3O signals in these experiments, a correction to the CH_3O profile had to be applied to account for it.

The solid lines through the experimental data are simulated CH_3O profiles, generated by numerical simulation of an assumed

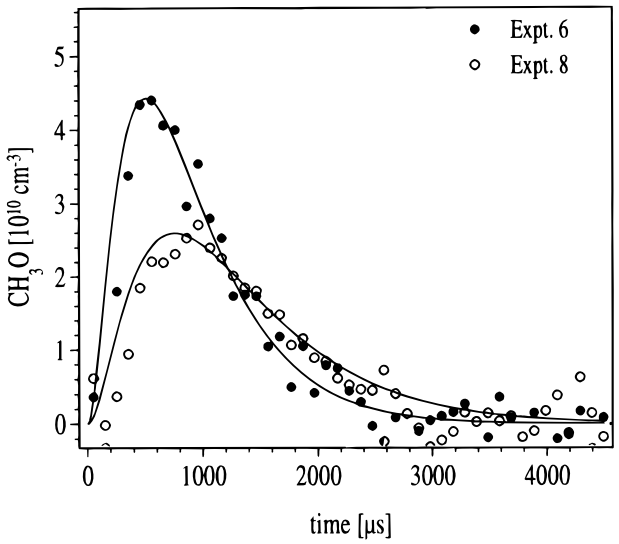

Figure 6. Formation and reaction of CH_3O in the 351 nm photolysis of $HONO/CH_3C(O)CH_3/NO_2$ mixtures at 20 Torr (Ar) and 297 K. The experimental conditions for each experiment can be taken from Table 3. Solid points are experiment 6; open symbols are experiment 8. The solid curves are the result of the numerical simulation using the reactions listed in Table 4 (apart from those labeled "other").

reaction scheme, which is listed in Table 4. The reaction scheme uses the data for the reactions of CH_3 and CH_3O with NO_2 measured as part of the present study. The simulations are able to reproduce the general features of the CH_3O formation and decay and the change in shape and concentration as experimental parameters such as the initial NO_2 and acetone concentration are changed. Although weak, the CH_3O signals and their time dependence are clearly good indicators of the formation and reaction of CH_3 in this system. The slight discrepancy between the measured rate of formation of the CH_3O and the modeled value is presumably due largely to errors associated with the calculated total loss rate of OH due to reaction with $CH_3C(O)CH_3$, NO_2, and HONO.

If we initially make the assumption that CH_3 is formed only in the title reaction, we can estimate branching ratios ($\alpha = k_{2a}/k_2$) to CH_3 formation by adjusting α (see Table 4) until the curves best fit the data points. The best fits were obtained with a branching ratio $\alpha(297\ K) = (0.5 \pm 0.15)$, where the errors simply reflect the variability of the fitted branching ratio between the three experiments. At 233 K the branching ratio obtained is $\alpha = (0.3 \pm 0.1)$. These values are also subject to large potential systematic errors related to the estimation of radical concentrations (both OH and CH_3O) by fluence measurements, although this error is somewhat reduced by the fact that the same Joulemeter at the same laser wavelength was used to estimate both OH and CH_3O concentrations. Large errors are also associated with the indirect method of determining the CH_3

TABLE 4: Reaction Scheme Used To Model the CH_3O Profiles in the OH + $CH_3C(O)CH_3$ + NO_2 Experiments

	k(233 K)	k(297 K)	note
	Reactions of OH		
$OH + CH_3C(O)CH_3 \rightarrow CH_3C(O)CH_2 + H_2O$	$(1.3 \times 10^{-13})\alpha$	$(1.7 \times 10^{-13})\alpha$	*a*
$OH + CH_3C(O)CH_3 \rightarrow CH_3 + CH_3C(O)OH$	$(1.3 \times 10^{-13})(1-\alpha)$	$(1.7 \times 10^{-13})(1-\alpha)$	*a*
$OH + HONO \rightarrow H_2O + NO_2$	3.4×10^{-12}	4.8×10^{-12}	*b*
$OH + NO_2 + M \rightarrow HNO_3 + M$	3.4×10^{-12}	1.2×10^{-12}	*b*
$OH + NO + M \rightarrow HONO + M$	9.3×10^{-13}	4.1×10^{-13}	*b*
	Reactions of Alkyl Radicals		
$CH_3C(O)CH_2 + NO_2 \rightarrow$ products	1.6×10^{-11}	1.6×10^{-11}	*c*
$CH_3C(O)CH_2 + NO \rightarrow$ products	2.6×10^{-11}	2.6×10^{-11}	*c*
$CH_3 + NO_2 \rightarrow CH_3O + NO$	1.91×10^{-11}	1.91×10^{-11}	this work
$CH_3 + NO_2 + M \rightarrow CH_3NO_2 + M$	3.43×10^{-11}	2.54×10^{-11}	this work
$CH_3 + NO + M \rightarrow CH_3NO + M$	2.8×10^{-12}	1.4×10^{-12}	*d*
	Reactions of CH_3O		
$CH_3O + NO_2 + M \rightarrow CH_3ONO_2 + M$	1.69×10^{-11}	7.62×10^{-12}	this work
$CH_3O + NO_2 \rightarrow$ products	6.9×10^{-14}	2.0×10^{-13}	*e*
$CH_3O + NO + M \rightarrow CH_3ONO + M$	1.1×10^{-11}	5.1×10^{-12}	*b*
$CH_3O + NO \rightarrow HCHO + HNO$	3.8×10^{-12}	3.0×10^{-12}	*f*
	Other		
$O + NO_2 \rightarrow NO + O_2$	1.1×10^{-11}	9.7×10^{-12}	*b*
$CH_3C(O)CH_2O \rightarrow CH_3CO + HCHO$	2×10^5	2×10^5	*g*
$CH_3C(O)CH_2O + NO_2 + M \rightarrow CH_3C(O)CH_2ONO_2 + M$			*h*
$CH_3CO + NO_2 \rightarrow CH_3 + CO_2 + NO$	2.5×10^{-11}	2.5×10^{-11}	*i*

[a] Temperature-dependent rate coefficient from Wollenhaupt et al.[8] [b] Temperature/pressure-dependent rate coefficients calculated for 20 Torr using JPL[22] parametrization. [c] Data at room temperature only from Sehested et al.[34] There are no measurements of this parameter at low temperatures. [d] Data for the low-pressure third-order rate coefficient provided by Davies et al.[36] was used to calculate k at 20 Torr of Ar. [e] McCaulley et al., 1985.[25] [f] McCaulley et al., 1990.[31] [g] Jenkin et al.[35] measured a decomposition frequency of $>1 \times 10^6$ s^{-1} at 298 K and 700 Torr of N_2, which broadly agrees with the estimation of Baldwin[37] of 8×10^6 s^{-1}. The value used is corrected for the pressure of 20 Torr in the present experiments. [h] Assumed to be the same as $CH_3O + NO_2 + M \rightarrow CH_3ONO_2 + M$. [i] Value obtained at room-temperature only,[38] and assumes immediate decomposition of the initially formed CH_3CO_2 product to form CH_3 and CO_2.

concentration and the need to calculate the partitioning of OH to a number of reactants such as $CH_3C(O)CH_3$, NO_2, HONO, and NO, although this error is reduced somewhat by making optical measurements of all of the species.

The trend in branching ratio with temperature is contrary to that expected if CH_3 is formed in reaction 2a via an association complex, the stabilization of which should be more favorable at low temperature.[8] This result can be understood if the decomposition of the vibrationally excited association complex, $[(CH_3)_2C(OH)O]$, proceeds either partially or completely via formation of an alkoxy radical:

$$OH + CH_3C(O)CH_3 \rightarrow [(CH_3)_2C(OH)O] \rightarrow (CH_3)_2C(OH)O \quad (9)$$

where $(CH_3)_2C(OH)O$ is the α-hydroxyisopropoxy radical, which can either decompose via C−C bond fission to form $CH_3C(O)OH + CH_3$ or react with NO_2 to form a nitrate:

$$(CH_3)_2C(OH)O + M \rightarrow CH_3 + CH_3C(O)OH + M \quad (10)$$

$$(CH_3)_2C(OH)O + NO_2 + M \rightarrow (CH_3)_2C(OH)ONO_2 + M \quad (11)$$

As the decomposition rate of the alkoxy radical will be strongly dependent on temperature (decreases with decreasing temperature), it is reasonable to assume that the competition between reactions 10 and 11 will favor nitrate formation at low temperatures, and the apparent yield of CH_3 will decrease. On the basis of the known concentration of NO_2 of $\approx 2 \times 10^{14}$ cm^{-3} and an estimated rate coefficient for reaction 14 of $\approx 4 \times 10^{-11}$ cm^3 s^{-1}, we estimate a loss rate of $(CH_3)_2C(OH)O$ of ≈ 8000 s^{-1} due to reaction with NO_2. The decomposition frequency of $(CH_3)_2C(OH)O$ at 20 Torr would have to be of a similar magnitude to compete, though, as far as we are aware, there are no measurements of this constant. The fate of alkoxy radicals in the atmosphere is either reaction with oxygen, decomposition or rearrangement.[33] For $(CH_3)_2C(OH)O$ the rearrangement pathway is precluded as this is accessible only to longer chain alkoxy radicals. There are also no H-atoms on the carbonyl C-atom that can be abstracted by reaction with O_2, and the fate in the atmosphere (where NO_2 is not available at the concentrations employed in the laboratory work) will probably be decomposition.

One further explanation for the present observation of a decreasing CH_3 yield with decreasing temperature, which we have already touched upon, is that the bimolecular rate coefficient for the reaction of $CH_3 + NO_2$ is significantly lower at 233 K than at 298 K, meaning that more CH_3 is converted to CH_3NO_2 and less is transformed to detectable CH_3O (see above). Neither the present data on the $CH_3 + NO_2$ reaction at pressures of 10 Torr or more nor the literature data have accurately established the temperature dependence of k_{3a}. The reaction of NO_2 with H-atoms has some similarity with the bimolecular component of the reaction of CH_3 with NO_2 as both reactions may be considered O-atom transfer to form NO and a further oxygen-containing radical:

$$H + NO_2 \rightarrow OH + NO \quad (12)$$

This reaction has a rate coefficient described by $k_{12} = 4.0 \times 10^{-10} \exp(-340/T)$ cm^3 s^{-1} [22] and thus displays a weak temperature dependence. We therefore examined the effect of fitting all the data in Figure 4 to $k_3 = k_{3a}(T) + k_{3b}(M,T)$, where $k_{3a}(T) = 4.5 \times 10^{-11} \exp(-250/T)$ cm^3 s^{-1}. These parameters were chosen to reproduce the room-temperature rate coefficient of 1.9×10^{-11} cm^3 s^{-1} for k_{3a} but remain within the limits we set for the variation with temperature given above (i.e., less than $-300/T$). The global fits thus obtained are not significantly different from those obtained with a temperature-independent

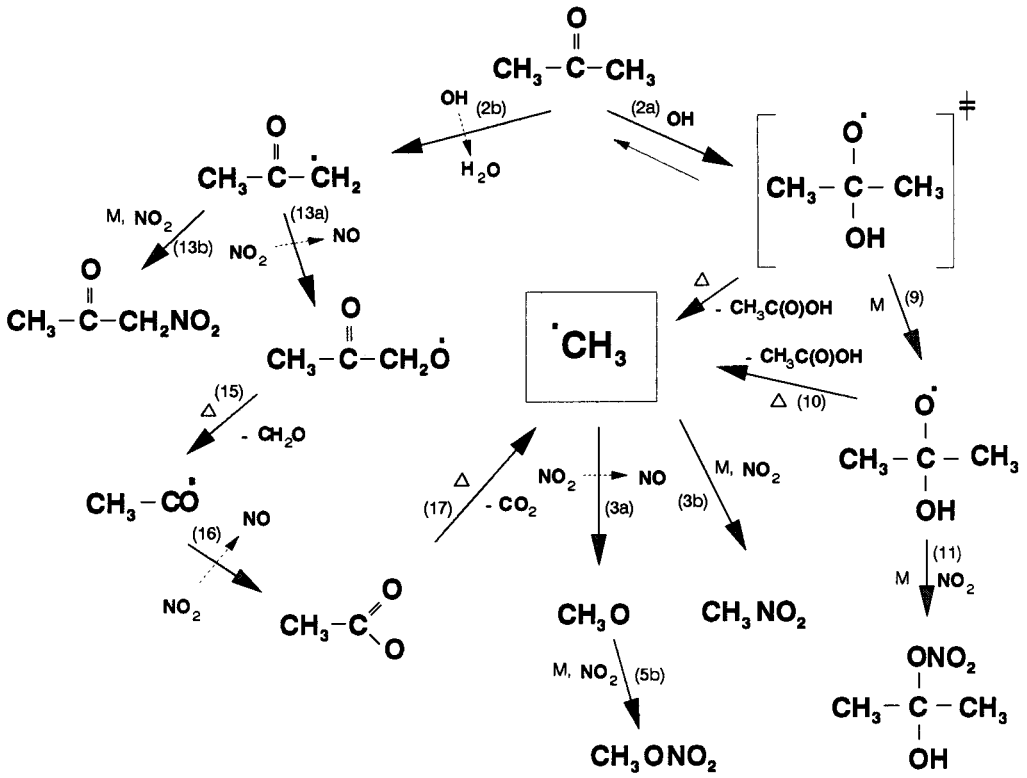

Figure 7. Schematic diagram illustrating the reactions studied and considered in the present work. The species in brackets is the association complex, which may have some characteristics of a vibrationally excited alkoxy radical. The numbers adjacent to the arrows represent the reaction numbers as given in the text.

rate coefficient of $k_{3a} = 1.9 \times 10^{-11}$ cm^3 s^{-1}. However, at low temperatures and 20 Torr, the ratio of k_{3b}/k_3 increases to almost 0.7 and the conversion of CH_3 to CH_3O is less efficient. This results in an underestimation of the branching to CH_3 at low temperatures.

Finally, we also consider the possibility that CH_3 can be formed in reactions of the acetonyl radical ($CH_3C(O)CH_2$) formed in the abstraction reaction of OH with $CH_3C(O)CH_3$ (2b):

$$OH + CH_3C(O)CH_3 \rightarrow CH_3C(O)CH_2 + H_2O \quad (2b)$$

The acetonyl radical is known[34] to react with NO_2 (13) and NO (14):

$$CH_3C(O)CH_2 + NO_2 \rightarrow CH_3C(O)CH_2O + NO \quad (13a)$$

$$CH_3C(O)CH_2 + NO_2 + M \rightarrow CH_3C(O)CH_2NO_2 + M \quad (13b)$$

$$CH_3C(O)CH_2 + NO + M \rightarrow CH_3C(O)CH_2NO + M \quad (14)$$

The α-carbonylalkoxy radical $CH_3C(O)CH_2O$ formed in reaction 13a is expected to decompose readily[35] to form the acetyl radical and HCHO (15). The fate of the acetyl radical in these experiments is reaction with NO_2 to form CH_3CO_2 which will unimolecularly decompose to form CH_3 radicals:

$$CH_3C(O)CH_2O + M \rightarrow CH_3CO + HCHO + M \quad (15)$$

$$CH_3CO + NO_2 \rightarrow CH_3CO_2 + NO \quad (16)$$

$$CH_3CO_2 + M \rightarrow CH_3 + CO_2 + M \quad (17)$$

Any CH_3 radicals formed in this sequence will react with NO_2 to form CH_3NO_2 and CH_3O which would result in an erroneous estimation of the yield of CH_3 from reaction 2.

The results of Sehested et al.[34] indicate that the reaction between $CH_3C(O)CH_2$ and NO_2 does not have a significant reaction pathway to form the α-carbonylalkoxy radical under their experimental conditions (1000 mbar of total pressure, mainly SF_6), implying that the reaction proceeds predominantly via a termolecular pathway to form $CH_3C(O)CH_2NO_2$ (13b).

However, this might not reflect the situation at 20 Torr, and to estimate the potential formation of CH_3 via this mechanism, we carried out numerical simulations of the reaction scheme in Table 4, in this case including the reactions designated "other" and assuming a worse-case scenario in which the reaction of $CH_3C(O)CH_2$ with NO_2 always generates $CH_3C(O)CH_2O$, i.e., $k_{13a}/k_{13} = 1$. A detailed reaction scheme of this chemistry and other reactions studied as part of the present investigations is given in Figure 7. We found that the variation in the CH_3O signal with experimental parameters could not be simulated by assuming CH_3 formation in reactions of $CH_3C(O)CH_2$ only. Generally the formation of CH_3 from reactions 2b, 13a, and 15−17 and the conversion of CH_3 to CH_3O was delayed by 400−500 μs relative to the observed signal, even if the decomposition of $CH_3C(O)CH_2O$ was assumed to be 1×10^6 s^{-1} (as measured at atmospheric pressure). This is due to the need for two reactions with NO_2 (one by $CH_3C(O)CH_2$ and one by CH_3CO) to form the CH_3 radical (see reaction scheme in Table 4). The results of this simulation (Figure 8) clearly show that CH_3 cannot arise solely from secondary reactions of the $CH_3C(O)CH_2$ radical. We therefore conclude that CH_3 is formed directly in the reaction of OH radicals with $CH_3C(O)CH_3$ and with a yield of ≈50% at room temperature, though the indirect nature of the present experiments does not allow us to place a

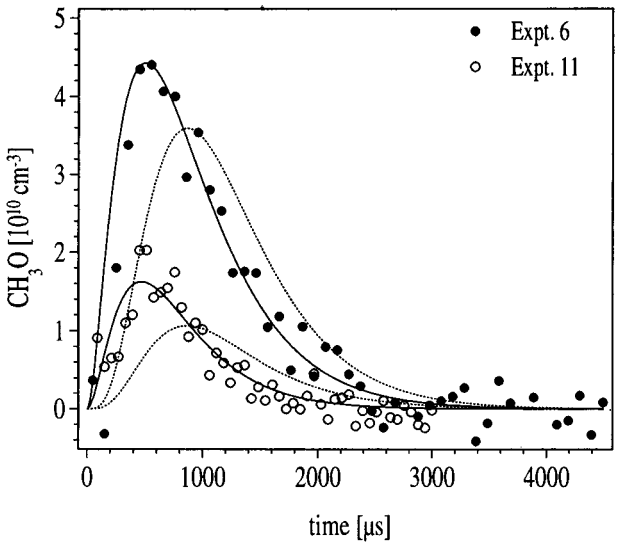

Figure 8. Numerical simulation of the CH_3O profiles using reaction 2b as CH_3 source (solid lines) and using the formation and reactions of $CH_3C(O)CH_2$ and $CH_3C(O)CH_2O$ in the presence of NO_2 as CH_3O source (broken lines, see text). Solid circles, data gathered at 297 K (experiment 6); open circles, data gathered at 233 K (experiment 11).

firm number on this branching ratio, and especially the temperature dependence of this process.

4. Conclusions

We have investigated the reactions of CH_3 and CH_3O with NO_2 under a variety of conditions of temperature and pressure and derived a parametrization of the rate coefficients of these reactions, which proceed by both pressure-dependent and pressure-independent pathways. The reaction of CH_3 with NO_2 was found to have a large contribution from a pressure-dependent term, even at pressures of less than 10 Torr. The termolecular rate coefficient in the limit of low pressure is given by $k_3^0 = (3.2 \pm 1.3) \times 10^{-28}(T/297)^{-0.3}$ cm^6 s^{-1}. The rate coefficient at the high-pressure limit is given by $k_3^\infty = (4.3 \pm 0.4) \times 10^{-11}(T/297)^{-1.2}$ cm^3 s^{-1}. An extrapolation of our results to 1 Torr yields a total rate coefficient of close to 2.5×10^{-11} cm^3 s^{-1}, in good agreement with previous low-pressure studies. The bimolecular reaction channel to give $CH_3O + NO$ has a rate coefficient of close to 1.9×10^{-11} cm^3 s^{-1}. For $CH_3O + NO_2$ the data are well simulated by $k_5^0 = (5.3 \pm 0.3) \times 10^{-29}(T/297)^{-4.4}$ cm^6 s^{-1} and $k_5^\infty = (1.9 \pm 0.05) \times 10^{-11}(T/297)^{-1.9}$ cm^3 s^{-1}. The hypothesized formation of significant amounts of CH_3 in the reaction of OH with $CH_3C(O)CH_3$ could be confirmed in the present work. A room-temperature branching ratio of 0.5 was established, though this result is associated with large uncertainty. Direct measurements of CH_3 formation in the reaction of OH with $CH_3C(O)CH_3$ would be most useful to resolve this issue.

References and Notes

(1) Singh, H. B.; O'Hara, D.; Herlth, D.; Sachse, W.; Blake, D. R.; Bradshaw, J. D.; Kanakidou, M.; Crutzen, P. J. *J. Geophys. Res.* **1994**, *99*, 1805.

(2) Singh, H. B.; Kanakidou, M.; Crutzen, P. J.; Jacob, D. J. *Nature* **1995**, *378*, 50.

(3) Arnold, F.; Bürger, V.; Droste-Fanke, B.; Grimm, F.; Krieger, A.; Schneider, J.; Stilp, T. *Geophys. Res. Lett.* **1997**, *24*, 3017.

(4) Jaeglé, L.; Jacob, D. J.; Wennberg, P. O.; Spivakovsky, C. M.; Hanisco, T. F.; Lanzendorf, E. J.; Hintsa, E. J.; Fahey, D. W.; Keim, E. R.; Proffitt, M. H.; Atlas, E. L.; Flocke, F.; Schauffler, S.; McElroy, C. T.; Midwinter, C.; Pfister, L.; Wilson, J. C. *Geophys. Res. Lett.* **1997**, *24*, 3181.

(5) Jaeglé, L.; Jacob, D. J.; Brune, W. H.; Tan, D.; Faloona, I. C.; Weinheimer, A. J.; Ridley, B. A.; Campos, T. L.; Sachse, G. W. *Geophys. Res. Lett.* **1998**, *25*, 1709.

(6) Folkins, I.; Chatfield, R.; Singh, H.; Chen, Y.; Heikes, B. *Geophys. Res. Lett.* **1998**, *25*, 1305.

(7) Wennberg, P. O.; Hanisco, T. F.; Jaeglé, L.; Jacob, D. J.; Hintsa, E. J.; Lanzendorf, E. J.; Anderson, J. G.; Gao, R.-S.; Keim, E. R.; Donnelly, S. G.; Del Negro, L. A.; Fahey, D. W.; McKeen, S. A.; Salawitch, R. J.; Webster, C. R.; May, R. D.; Herman, R. L.; Proffitt, M. H.; Margitan, J. J.; Atlas, E. L.; Schauffler, S. M.; Flocke, F.; McElroy, C. T.; Bui, T. P. *Science* **1997**, *279*, 49.

(8) Wollenhaupt, M.; Carl, S. A.; Horowitz, A.; Crowley, J. N. *J. Phys. Chem. A* **2000**, *104*, 2695.

(9) Jacob, D. J.; Heikes, B. G.; Fan, S.-M.; Logan, J. A.; Mauzerall, D. L.; Bradshaw, J. D.; Singh, H. B.; Gregory, G. L.; Talbot, R. W.; Blake, D. R.; Sachse, G. W. *J. Geophys. Res.* **1996**, *101*, 24235.

(10) Flocke, F.; Atlas, E.; Madronich, S.; Schauffler, S. M.; Aikin, K.; Margitan, J. J.; Bui, T. P. *Geophys. Res. Lett.* **1998**, *25*, 1891.

(11) Smith, I. W. M. *J. Chem. Soc., Faraday Trans.* **1991**, *87*, 2271.

(12) Inoue, G.; Akimoto, H.; Okuda, M. *J. Chem. Phys.* **1980**, *72*, 1769.

(13) Wantuck, P. J.; Oldenborg, R. C.; Baughcum, S. L.; Winn, K. R. *J. Phys. Chem.* **1987**, *91*, 3253.

(14) Bongartz, A.; Kames, J.; Welter, F.; Schurath, U. *J. Phys. Chem.* **1991**, *95*, 1076.

(15) Bongartz, A.; Kames, J.; Schurath, U.; George, C.; Mirabel, P.; Ponche, J. L. *J. Atmos. Chem.* **1994**, *18*, 149.

(16) Lightfoot, P. D.; Kirwan, S. P.; Pilling, M. J. *J. Phys. Chem.* **1988**, *92*, 4938.

(17) Donaldson, D. J.; Leone, S. R. *J. Phys. Chem.* **1987**, *91*, 3128.

(18) Taylor, W. D.; Allston, T. D.; Moscato, M. J.; Fazekas, G. B.; Kozlowski, R.; Takacs, G. A. *Int. J. Chem. Kinet.* **1980**, *12*, 231.

(19) Cox, R. A.; Derwent, R. G.; Kearsey, S. V.; Batt, L.; Patrick, K. G. *J. Photochem.* **1980**, *13*, 149.

(20) Lake, J. S.; Harrison, A. J. *J. Chem. Phys.* **1959**, *30*, 361.

(21) Schneider, W.; Moortgat, G. K.; Tyndall, G. S.; Burrows, J. P. *J. Photochem. Photobiol.* **1987**, *40*, 195.

(22) DeMore, W. B.; Sander, S. P.; Golden, D. M.; Hampson, R. F.; Kurylo, M. J.; Howard, C. J.; Ravishankara, A. R.; Kolb, C. E.; Molina, M. J. *Chemical Kinetics and Photochemical Data for Use in Stratospheric Modelling, No. 11*; Jet Propulsion Laboratory, 1997.

(23) Atkinson, R.; Baulch, D. L.; Cox, R. A.; Hampson, R. F. J.; Kerr, J. A.; Rossi, M. J.; Troe, J. *J. Phys. Chem. Ref. Data* **1997**, *26*, 1329.

(24) Troe, J. *J. Phys. Chem.* **1979**, *83*, 114.

(25) McCaulley, J. A.; Anderson, S. M.; Jeffries, J. B.; Kaufman, F. *Chem. Phys. Lett.* **1985**, *115*, 180.

(26) Biggs, P.; Canosa-Mas, C. E.; Fracheboud, J.-M.; Parr, A. D.; Shallcross, D. E.; Wayne, R. P. *J. Chem. Soc., Faraday Trans.* **1993**, *89*, 4163.

(27) Frost, M. J.; Smith, I. W. M. *J. Chem. Soc., Faraday Trans.* **1990**, *86*, 1751.

(28) Frost, M. J.; Smith, I. W. M. *J. Chem. Soc., Faraday Trans.* **1990**, *86*, 1757.

(29) Glänzer, K.; Troe, J. *Ber. Bunsen-Ges. Phys. Chem.* **1974**, *78*, 182.

(30) Yamada, F.; Slagle, I. R.; Gutman, D. *Chem. Phys. Lett.* **1981**, *83*, 409.

(31) McCaulley, J. A.; Moyle, A. M.; Golde, M. F.; Anderson, S. M.; Kaufman, F. *J. Chem. Soc., Faraday Trans.* **1990**, *86*, 4001.

(32) Park, J.-Y.; Gutman, D. *J. Phys. Chem.* **1983**, *87*, 1844.

(33) Atkinson, R. *Int. J. Chem. Kinet.* **1997**, *29*, 99.

(34) Sehested, J.; Christensen, L. K.; Nielsen, O. J.; Bilde, M.; Wallington, T. J.; Schneider, W. F.; Orlando, J. J.; Tyndall, G. S. *Int. J. Chem. Kinet.* **1998**, *30*, 475.

(35) Jenkin, M. E.; Cox, R. A.; Emrich, M.; Moortgat, G. K. *J. Chem. Soc., Faraday Trans.* **1993**, *89*, 2983.

(36) Davies, K. W.; Green, N. J. B.; Pilling, M. J. *J. Chem. Soc., Faraday Trans.* **1991**, *87*, 2317.

(37) Baldwin, A. C.; Barker, J. R.; Golden, D. M.; Hendry, D. G. *J. Phys. Chem.* **1977**, *81*, 2483.

(38) Slagle, I. R.; Gutman, D. *J. Am. Chem. Soc.* **1981**, *104*, 4741.